Acta Crystallographica Section D
Biological Crystallography
ISSN 0907-4449

Single-wavelength anomalous diffraction phasing revisited

Luke M. Rice,[a] Thomas N. Earnest[b] and Axel T. Brunger[c]*

[a]Department of Molecular Biophysics and Biochemistry, Yale University, New Haven, CT 06520, USA, [b]Macromolecular Crystallography Facility at the Advanced Light Source, Physical Biosciences Division, Lawrence Berkeley National Laboratory, Berkeley, CA 94720, USA, and [c]Howard Hughes Medical Institute and Departments of Molecular and Cellular Physiology, Neurology and Neurological Science and Stanford Synchrotron Radiation Laboratory, Stanford University, Stanford, CA 94305, USA

Correspondence e-mail: axel.brunger@stanford.edu

Received 18 May 2000
Accepted 19 July 2000

Multiwavelength anomalous diffraction (MAD) phasing has become a routinely used tool for determining new macromolecular structures. The MAD method has stringent data-collection requirements, typically necessitating radiation-resistant crystals and access to a tunable synchrotron beamline. In cases where synchrotron time, monochromator tunability or radiation damage is a concern or where high-throughput structure determination is desired, phasing methods capable of producing interpretable electron-density maps from less data become attractive alternatives to MAD. The increasing availability of tunable synchrotron data-collection facilities prompted the authors to revisit single-wavelength anomalous diffraction (SAD) phasing used in conjunction with a phase-ambiguity resolving method such as solvent flattening. The anomalous diffraction from seven different selenomethionine-labelled protein crystals has been analysed and it is shown that in conjunction with solvent flattening, diffraction data from the peak anomalous wavelength alone can produce interpretable electron-density maps of comparable quality to those resulting from full MAD phasing. Single-wavelength anomalous diffraction (SAD) phasing can therefore be a time-efficient alternative to MAD. The data also show that radiation damage can have a significant effect on the quality of SAD/MAD diffraction data. These results may be useful in the design of optimal strategies for collection of the diffraction data.

1. Introduction

As early as 1985, it was predicted that most new structures would be solved by combining density-modification techniques with phasing by single isomorphous replacement (SIR) or by single-wavelength anomalous diffraction (SAD; Wang, 1985). A survey of the macromolecular structures database (Hendrickson & Wüthrich, 1991–1999; http://www.biomednet.com/db/msd/) shows that this prediction has not yet come to pass. Only a limited number of macromolecular structures have been solved using SIR or SAD data. In place of these techniques, the multiwavelength anomalous diffraction (MAD) method (Hendrickson, 1991) has risen to a position of prominence among experimental phasing methods (Ogata, 1998).

In the absence of other crystallographic phase information, anomalous diffraction data collected at a single wavelength cannot produce unimodal phase-probability distributions. This inability to provide unique phase choices is termed the SAD phase ambiguity and electron-density maps computed using SAD phases are generally difficult, if not impossible, to

Table 1
Experimental details of the data used in the phasing tests.

Phasing ratio denotes denotes the macromolecular weight contained in the asymmetric unit divided by the number of Se atoms in the asymmetric unit. R.m.s. ΔF corresponds to the root-mean-square anomalous differences in the diffraction data, computed from the formula $\langle||F^+| - |F^-||^2\rangle^{1/2} / \left[\left(\langle||F^+| - |F^-||^2\rangle\right)/2\right]^{1/2}$, where F^+ and F^- denote a Friedel pair. Data sets 1qqe and all the 1qcs data sets were collected at ALS beamline 5.0.2. Data sets 1zbd and 1kwa were collected at NSLS beamline X4A. Data sets 1sfc, 1edu and 1nsf were collected at SSRL beamline 1-5.

Test case	Resolution (Å)	Solvent content (%)	Phasing ratio (kDa)	$R_{\rm merge}$ (%)	Completeness (%)	Centric fraction (%)	Multiplicity	R.m.s. ΔF	I/σ_I	Peak wavelength (Å)
1sfc	3.3	55	2.2	10.8 (38.0)	97.4 (97.7)	5	3.5	0.137	11.3	0.9795
1qqe	3.3	70	10.3	7.0 (31.3)	99.8 (99.9)	5	3.9	0.064	18.7	0.98
1kwa	2.1	40	2.3	6.0 (14.0)	98.6 (94.2)	7	4.1	0.097	21.1	0.9791
1zbd	2.6	55	3.3	5.1 (39.6)	98.7 (97.9)	2	2.5	0.080	15.8	0.9789
1nsfd	2.4	56	3.7	6.4 (31.2)	89.0 (73.0)	4	2.8	0.089	9.6	0.9795
1edu	1.8	40	3.0	8.1 (43.7)	98.4 (89.0)	8	5.8	0.071	20.8	0.9796
1qcsa	1.9	50	8.0	6.0 (20.3)	97.8 (89.8)	7	3.6	0.062	21.3	0.9799
1qcsb	1.8	50	8.0	8.9 (37.0)	99.1 (96.9)	7	3.9	0.067	18.5	0.9795

interpret. The MAD method is currently the most popular technique used to resolve the SAD phase ambiguity and thereby obtain interpretable electron-density maps (Hendrickson & Wüthrich, 1991–1999; Ogata, 1998). In a MAD experiment, additional data are collected near the absorption edge of the anomalous scatterer and the differences between diffraction amplitudes at different wavelengths are used to obtain a unique phase choice (reviewed by Hendrickson & Ogata, 1997).

Collecting diffraction data for a MAD experiment can take as much as eight times longer than the collection of native or derivative data (reviewed by Walsh *et al.*, 1999). This disadvantage is offset by the fact that MAD typically uses measurements from a single crystal and hence does not suffer from the problems related to lack of isomorphism that can plague isomorphous replacement methods. Furthermore, the behavior of anomalous scattering with resolution is such that the signal arising from the anomalous scatterers becomes relatively more important with increasing resolution (Hendrickson & Ogata, 1997). In favorable cases, MAD phases can provide experimental electron-density maps of exceptional quality (Burling *et al.*, 1996).

The advantages of MAD have been well documented (Hendrickson & Ogata, 1997), but the fact that the method requires access to a tunable synchrotron beamline and extensive data collection from a single crystal are disadvantages worthy of comment. Indeed, while the success of the MAD method has given rise to the development of new dedicated synchrotron beamlines (SSRL 9-2, ALS 5.0.2, APS ID-19, ESRF BM14, to name a few), access to these beamlines remains a limiting factor for many research laboratories. The development of cryoprotection techniques (reviewed by Garman & Schneider, 1997) has greatly reduced the radiation sensitivity of most macromolecular crystals, but nevertheless in unfavorable cases radiation damage can cause a MAD experiment to fail (Rice & Brunger, 1999; Yu *et al.*, 1999). With the increasing availability of third-generation undulator synchrotron sources, the problem of radiation damage is likely to return to the foreground.

A number of recent studies have addressed these and other potential problems with MAD experiments by attempting to derive interpretable electron-density maps from fewer diffraction data. In theory, two suitably chosen wavelengths are sufficient to obtain unique experimental phases (Phillips & Hodgson, 1980). Practical guidelines for choosing these wavelengths so as to obtain the best possible phases have been presented (Gonzalez *et al.*, 1999) and phases thus obtained are generally sufficient to solve a structure. More strikingly, a return to the work of Hendrickson & Teeter (1981) has shown the feasibility of using the anomalous scattering of sulfur at Cu $K\alpha$ wavelength to solve macromolecular crystal structures (Dauter *et al.*, 1999). Furthermore, the possibility of phasing using a single wavelength and the anomalous scattering of ordered solvent bromide ions has also recently been demonstrated (Dauter & Dauter, 1999). Finally, another description of an application of high-resolution SAD phasing includes the use of the anomalous scattering from bound holmium or zinc ions (Brodersen *et al.*, 2000).

There have been recent developments in direct-methods phasing combined with SAD data that promise to resolve the SAD ambiguity without solvent flattening (Hauptman, 1996; Langs *et al.*, 1999). Most applications of SAD phasing, however, have used density-modification techniques to resolve the phase ambiguity (Hendrickson & Wüthrich, 1991–1999). When SAD phasing has been applied to the determination of previously unknown structures, non-crystallographic symmetry averaging has commonly been used in addition to solvent flattening (Hendrickson & Wüthrich, 1991–1999). Thus, there are not many examples of structures solved using only solvent flattening and SIR or SAD data. Recent examples of successful SAD phasing have elegantly demonstrated the potential power of the technique (Brodersen *et al.*, 2000; Dauter *et al.*, 1999; Dauter & Dauter, 1999). None of these studies used selenomethionine as the anomalous scatterer and all had relatively high resolution diffraction data available. It is thus appropriate to re-examine whether the combination of selenomethionine SAD and solvent flattening can provide a general phasing method over a broader range of moderate-resolution diffraction data.

In this work, we revisit the phasing of seven structures, all determined using anomalous scattering methods in conjunction with selenomethionine-labelled protein (Hendrickson *et al.*, 1990; Doublie, 1997). The seven cases vary considerably in terms of the size of the asymmetric unit (18–100 kDa), the solvent content (40–70%), the number of Se atoms, the centric fraction and the high-resolution limit of the diffraction (1.8–3.3 Å; Table 1). For each case, we used diffraction data from

the peak anomalous wavelength and performed SAD phasing followed by solvent flipping (Abrahams & Leslie, 1996; Abrahams, 1997) and histogram matching (Zhang & Main, 1990). Where applicable, the results of this SAD phasing procedure were compared with MAD phasing using all the available data. In nearly every case, the combination of selenomethionine SAD phasing with density modification would have been sufficient to unambiguously determine the structure. Based on our results and those of others, it appears that SAD phasing provides a broadly applicable method for determining new macromolecular structures.

2. Methods

The diffraction data used in this work were all obtained from three- or four-wavelength MAD experiments performed around the selenium edge at a number of different synchrotron beamlines (ALS 5.0.2, Brookhaven X4A, SSRL 1-5). The test cases will be referred to by the PDB code associated with the final refined structure. For five of the seven cases [1sfc (Sutton *et al.*, 1998), 1kwa (Daniels *et al.*, 1998), 1zbd (Ostermeier & Brunger, 1999), 1nsf (Yu *et al.*, 1998) and 1edu (Hyman *et al.*, 2000)], initial phases were determined by a combination of MAD phasing and density modification. For the other cases [1qcS (Yu *et al.*, 1999) and 1qqe (Rice & Brunger, 1999)], full MAD phasing failed owing to uncharacterized problems with the dispersive anomalous differences. The original phasing of 1qqe used only imaginary (f'') anomalous differences and that of 1qcs used imaginary (f'') anomalous differences supplemented with the weak dispersive anomalous differences between the peak anomalous and inflection point data. The peak anomalous wavelength is defined as the wavelength that gives rise to maximal selenium fluorescence, which was measured separately for every crystal.

For the 1qcs case, we have collected a number of additional data sets. The original 1qcs data (called 1qcsa in this work) used for the structure determination were from a three-wavelength MAD experiment collected one wavelength at a time. We re-performed a three-wavelength MAD experiment in which a small wedge of reciprocal space was collected at all three wavelengths before moving to the next wedge; both the original (1qcsa) and re-collected (1qcsb) data have been analyzed in this work. We also collected three complete data sets from a single crystal at the selenium peak anomalous wavelength; these data will be referred to as 1qcsc1, 1qcsc2 and 1qcsc3. Data sets 1qcsb, 1qcsc1, 1qcsc2 and 1qcsc3 were indexed using *HKL*2000 (Otwinowski & Minor, 1997) and integrated using *SCALEPACK* (Otwinowski & Minor, 1997).

For all cases, diffraction data were collected from a single cryoprotected crystal at 100 K. All data except for 1qcsa and 1qqe were collected in small wedges at all wavelengths before moving to the next wedge. In several cases (1sfc, 1nsf, 1qqe and 1kwa), native diffraction data were available to higher resolution than the MAD data; in the original structure determination the resolution limit of the experimental phases was extended by density modification. In the current work, no such phase extension was performed in order to simplify the analysis. All analysis was performed using only the MAD or SAD diffraction data.

All calculations after data processing were carried out using the *Crystallography & NMR System* (*CNS*; Brunger *et al.*, 1998). Phasing against MAD or SAD data used maximum-likelihood target functions as implemented in *CNS* (Burling *et al.*, 1996; Brunger *et al.*, 1998). Heavy-atom sites were taken from the original structure determination; in most cases these sites were obtained from automated Patterson searches using the peak anomalous data alone (Grosse-Kunstleve & Brunger, 1999). Log-likelihood gradient maps (Bricogne, 1984) were inspected to confirm that all anomalously scattering sites were accounted for. Initial SAD or MAD phases were improved using density modification, in particular by solvent flipping (Abrahams & Leslie, 1996; Abrahams, 1997) and histogram matching (Zhang & Main, 1990). Salient features of the test cases are summarized in Table 1. The test cases cover a wide range of commonly encountered experimental conditions.

SAD- and MAD-phased electron-density maps were compared using the map correlation coefficient, calculated in reciprocal space from the formula

$$\text{correlation} = \frac{\sum_{hkl} \text{fom}_i |F_i^{hkl}| \text{fom}_j |F_j^{hkl}| \cos(\varphi_i - \varphi_j)}{\left(\sum_{hkl} |\text{fom}_i F_i^{hkl}|^2 \sum_{hkl} |\text{fom}_j F_j^{hkl}|^2 \right)^{1/2}},$$

where fom denotes the figure of merit and $|F|$ and φ denote the structure-factor amplitude and phase, respectively. To assess the success of the phasing trials, figure-of-merit-weighted SAD and MAD electron-density maps, both before and after density modification, were compared with σ_A-weighted (Read, 1986) $2F_o - F_c$ electron-density maps calculated from the final refined model. Where applicable, SAD and MAD maps were compared with each other, also using the overall map correlation coefficient.

3. Results and discussion

The agreement of SAD or MAD electron-density maps with a σ_A-weighted $2F_o - F_c$ electron-density map computed from the final refined model is shown in Fig. 1(*a*). In general, before density modification MAD electron-density maps are considerably better than their SAD counterparts. This is expected: the use of data collected at multiple wavelengths should resolve the phase ambiguity inherent with the use of a single wavelength. It is important to note that anomalous data collected at a single wavelength cannot provide phase information about centric reflections. This does not appear to have given rise to any problems in our tests. Density modification will subsequently assign phases to these centric reflections.

There is considerable variation in the degree to which unmodified MAD electron-density maps agree with maps computed from the final refined model (Fig. 1*a*). Since all the test cases presented here used selenium as the anomalous scatterer, the relative contribution of real (f') and imaginary (f'') anomalous differences to the phasing should be constant. These differences in the quality of initial MAD phases prob-

ably reflect the degree to which the real or imaginary anomalous differences were reliably measured. For example, SAD phasing of the 1edu data gave surprisingly poor results, especially when compared with the MAD maps, which were of exceptional quality (Fig. 1*a*). This prompted us to re-examine the initial data processing; it appears that the crystal was mis-centered. The data for 1edu were collected using inverse-beam geometry, so this mis-centering introduced a systematic error into the measurement of the imaginary anomalous differences. This error did not effect the measurement of most of the dispersive anomalous differences, which probably explains why the MAD phasing was successful while the SAD phasing was not.

Density modification in the form of solvent flipping and histogram matching improves both the SAD and MAD phases, but has a more dramatic effect on the SAD phases. After density modification, SAD and MAD phases for 1nsf, 1kwa, 1zbd and 1qcsb were nearly indistinguishable (Fig. 1*b*). Furthermore, density-modified SAD phases for 1qcsa and 1qqe, for which MAD phasing failed, show very good correlation to the final refined model (Fig. 1*a*) and were in fact sufficient to determine the structure. Representative sections of density-modified SAD or MAD phases for 1nsf and 1kwa are shown side by side in Figs. 2(*a*) and 2(*c*), respectively. For the 1kwa case, density-modified SAD and MAD phases give rise to electron-density maps of reasonable quality, sufficient in both cases to trace most of the molecule. The 1kwa case (along with 1edu) has the lowest solvent content (40%) of all the test cases, demonstrating that high solvent content is not a prerequisite for using density modification to resolve the SAD phase ambiguity. Compared with 1kwa, the 1nsf case has a higher solvent content (60%) but a poorer phasing ratio and less complete, less redundant and less intense diffraction data. Nevertheless, the maps obtained from SAD phasing and density modification are similar to their MAD counterparts; both are of exceptional quality.

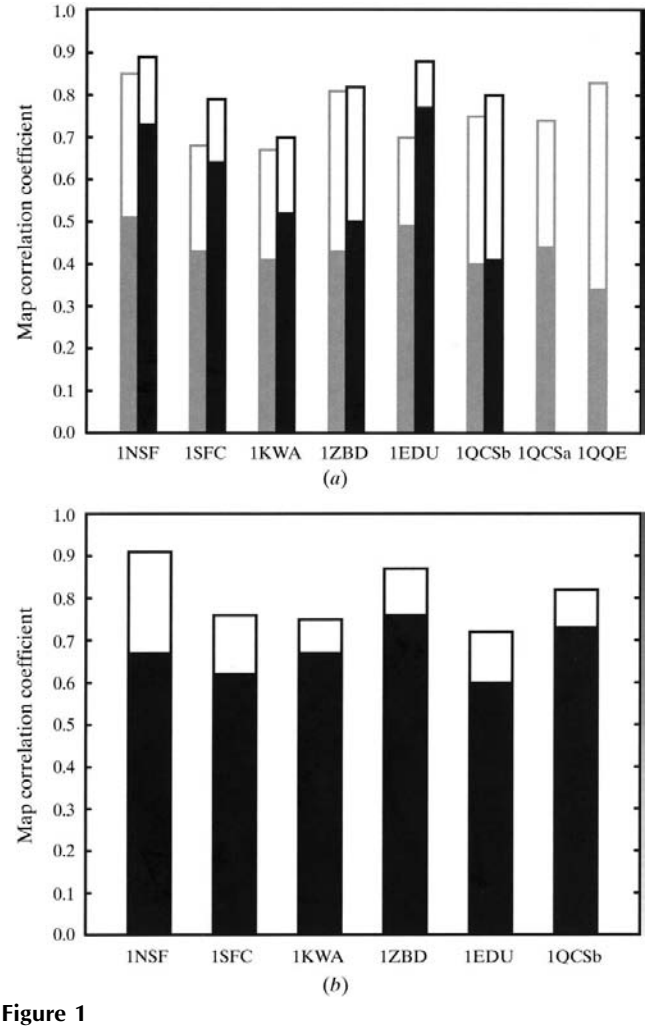

Figure 1
Evaluation of SAD- and MAD-phased electron-density maps before and after solvent flipping and histogram matching. (*a*) Correlation between SAD (grey) or MAD (black) electron-density maps and a σ_A-weighted $(2F_o - F_c)$ electron-density map computed from the final refined model. Filled bars correspond to unmodified maps; open bars denote maps after density modification. (*b*) Correlation between SAD and MAD electron-density maps before (solid bars) and after (open bars) density modification.

According to our tests, SAD phasing followed by density modification will usually be sufficient to determine a new structure. Our data also shows that maps calculated from density-modified MAD phases will be even better (Fig. 1*a*). To assess the quality of MAD or SAD phases as a function of resolution, we also plotted map correlation coefficients calculated in reciprocal space in equal volume resolution shells (Figs. 2*b* and 2*d*). Before density modification, MAD phases significantly outperform their SAD counterparts across the entire resolution range. After density modification, however, the difference between SAD and MAD phases is much smaller, especially at low to moderate resolution.

Aside from the 1edu case, in which the crystal was not centered in the beam, 1sfc represents the case in which density-modified SAD phases most deviated from their MAD counterparts. We believe that this is a consequence of the relatively poor quality of the diffraction data (Sutton *et al.*, 1998; Table 1) and not of an inherent limitation in the applicability of SAD phasing. Indeed, the peak anomalous data we used for 1sfc comes from crystals labelled with selenomethionine on three of the four polypeptides (data set Sn1Sn2Sx in the notation of Sutton *et al.*, 1998). This data combine a moderate diffraction limit (3.3 Å for the anomalous data) with relatively noisy (high $R_{\rm merge}$) and weak (low I/σ_I) data. When we used the peak anomalous data from a doubly labelled complex (data set Sn1Sn2; Sutton *et al.*, 1998), the difference between SAD and MAD phases after density modification was smaller (not shown). In the initial structure determination of 1sfc, multiple MAD experiments were performed in order to produce electron-density maps of excellent quality. A significant improvement in the quality of the density-modified phases occurred when SAD phases obtained from the doubly and triply labelled complexes were combined (not shown). Multiple SAD experiments using different sets of labels is thus an economic viable alternative to multiple MAD experiments in cases where experimental conditions limit the applicability of SAD alone.

Two of the seven structures used as test cases (1qqe and 1qcsa) were essentially solved using only density-modified SAD phases (see §2). These two cases have the most unfavorable selenium content and represent the highest (1qcsa) and lowest (1qqe) resolution diffraction. A representative section of the density-modified SAD electron-density map for 1qqe is shown in Fig. 3. The electron density, obtained at the moderate resolution of 3.3 Å, is notable considering that the 33 kDa structure was phased with only three Se atoms, all of which had *B* factors of near 100 Å^2.

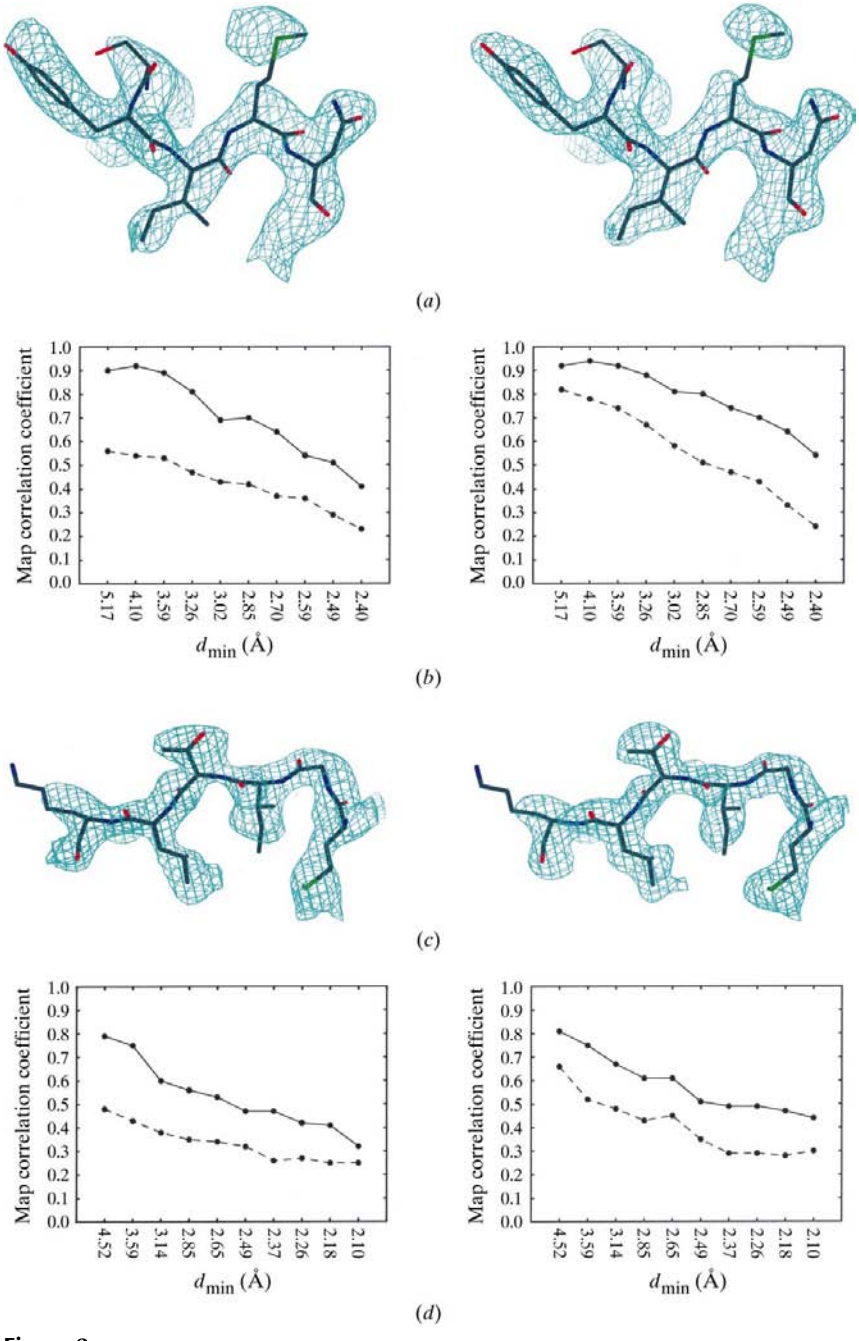

Figure 2
Representative electron density from density-modified SAD and MAD maps for two of the test cases and analysis of the maps as a function of resolution. (*a*) Test case 1nsf. Density-modified SAD (left) and MAD (right) maps are very similar and of good quality. Maps were calculated to 2.4 Å resolution and are contoured at 1.25σ. The final refined model is shown in a stick representation. (*b*) Test case 1nsf. Correlation coefficients (in ten equal volume resolution shells) between the σ_A-weighted ($2F_o - F_c$) electron-density map computed from the final refined model and SAD (left) and MAD (right) maps before (dashed line) and after (solid line) density modification. (*c*) Test case 1kwa. Again, SAD and MAD maps are very similar, although of lesser quality than for 1nsf. Electron-density maps were calculated to 2.1 Å resolution and are contoured at 1.25σ. The final refined model is shown in a stick representation. (*d*) Test case 1kwa. As for (*b*).

The nature and extent of radiation damage suffered by macromolecular crystals upon prolonged exposure to synchrotron radiation has recently been investigated (Weik *et al.*, 2000; Ravelli & McSweeney, 2000; Burmeister, 2000). The effect(s) of radiation damage on a MAD or SAD experiment have not yet been as comprehensively assessed. As a first step toward this goal, we collected three SAD data sets (from the same crystal) at the SeMet anomalous peak wavelength using the 1qsc crystals. Each of these data sets (1qcsc1, 1qcsc2 and 1qcsc3) covered an identical total oscillation range and used identical exposure times. The total time in the X-ray beam is comparable to that required for a full MAD experiment, so any radiation decay observed would be relevant to a MAD analysis. Relevant parameters describing these data sets are summarized in Table 2. There is clear evidence of radiation decay as evidenced by a loss of high-resolution diffraction and an increase in R_{merge}.

In spite of increasing radiation damage, each of the three data sets was sufficient to identify the selenium sites using automated Patterson searching as implemented in *CNS* (Grosse-Kunstleve & Brunger, 1999) (not shown). The effects of radiation damage became apparent after SAD phasing using each data set (Table 2 and Fig. 4). Refinement of the selenium positions yielded progressively higher *B* factors in subsequent data sets (Table 2), confirming the increasing extent of radiation damage. There are small but consistent differences between electron-density maps computed from 1qcsc1 and 1qcsc2, and both of these maps are significantly better than the map computed from 1qcsc3 (Fig. 4). These phasing calculations were performed using a number of different high-resolution limits (1.8, 2.0, 2.25 and 2.5 Å) in order to probe the extent and resolution dependence of the damage arising from the increasing dose of radiation. Differences between SAD phases derived from 1qcsc1 and 1qcsc2 are readily apparent only using the highest resolution diffraction data. In contrast, even when the data were truncated to 2.5 Å resolution, phases derived

Table 2
1qcsc diffraction data.

Statistical parameters describing three SAD data sets taken from the same crystal at a wavelength of 0.9795 Å. Diffraction data were processed using a number of different high-resolution limits. Se *B* factor denotes the average *B* factor of the selenium sites after SAD refinement. Map correlation denotes the overall map correlation coefficient between the solvent-flattened SAD electron-density map and a σ_A-weighted $2F_o - F_c$ electron-density map computed from the final refined model. These data sets were collected at ALS beamline 5.0.2.

Resolution limit (Å)	1.8			2.0			2.25			2.5		
Data set	1	2	3	1	2	3	1	2	3	1	2	3
R_{sym}	7.9	10.1	12.3	7.0	8.1	11.5	6.2	6.6	8.8	5.9	6.0	7.6
I/σ_I	20.9	16.8	11.3	23.8	20.1	15.0	25.7	24.2	19.3	26.7	26.1	22.6
Mosaicity	0.48	0.63	0.78	0.48	0.63	0.78	0.48	0.63	0.78	0.48	0.63	0.78
Se *B* factor	26	46	134	26	45	114	29	42	80	32	43	78
Map correlation	0.81	0.74	0.40	0.78	0.74	0.45	0.74	0.74	0.58	0.72	0.73	0.60

from data set 1qcsc3 are markedly poorer than those from earlier data sets. The degree to which the phasing is adversely affected by radiation damage is probably case-dependent and is likely to depend on the environment of the anomalous scattering sites.

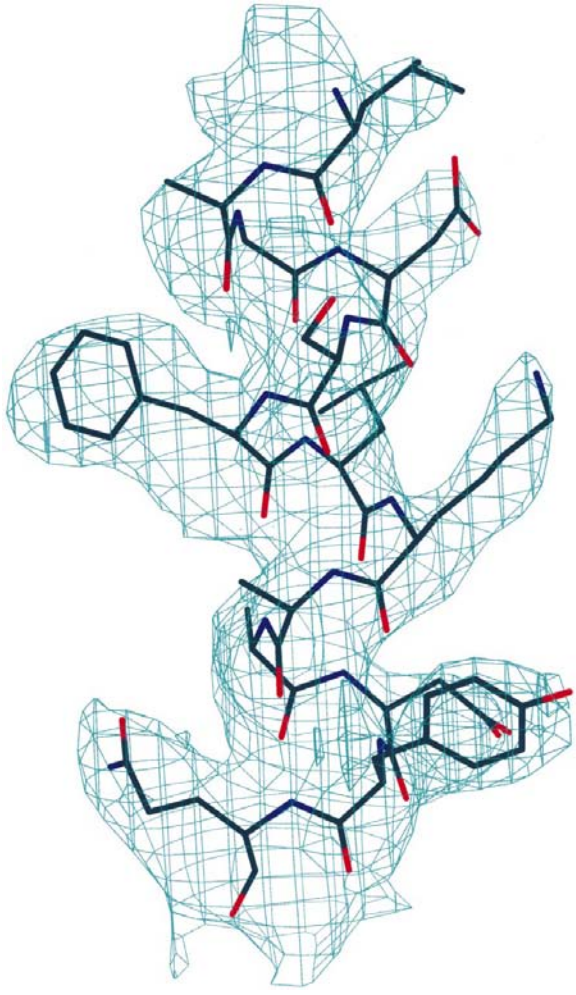

Figure 3
Representative electron density from the density-modified SAD map for test case 1qqe. The map was calculated at 3.3 Å resolution and is contoured at 1.25σ. This test case combines the poorest diffraction limit with the smallest anomalous signal.

Many of the data sets used in this work were collected with the intention of using MAD phasing. We and others frequently collect MAD data in wedge mode, which entails collecting a small (typically 15–20°) wedge of diffraction data at each wavelength before moving on to the next wedge of data. This strategy is designed to minimize systematic errors in the measurement of both real and imaginary anomalous differences, but it represents a compromise where the measurement of imaginary (f'') anomalous differences is concerned. Data sets 1nsf, 1edu, 1kwa, 1sfc and 1zbd were collected in this manner and it is likely that the accurate measurement of the imaginary anomalous differences was to some degree negatively affected by the data-collection strategy. Given that in one case (1qcs) we observed significant radiation damage on the time scale of a MAD experiment, we expect that SAD phases derived from data sets 1nsf, 1edu, 1kwa, 1sfc and 1zbd all suffer from radiation damage to varying extents. Data sets 1qcs and 1qqe were collected one wavelength at a time (peak anomalous wavelength first) and therefore represent more optimally measured SAD data.

4. Conclusions

The data presented here allow us to make a number of recommendations regarding phasing and data-collection strategy. In all of our calculations, MAD phases are better than SAD phases, both before and after density modification. Thus, under conditions where crystal robustness and data-collection instrumentation are not limited or under conditions where extremely accurate experimental phases are required (Burling *et al.*, 1996), it is advisable to perform a full MAD experiment. However, our phasing trials also show that for selenomethionine-labelled crystals data collected at the peak anomalous wavelength will generally be sufficient to determine a new structure from crystals having a broad range of high-resolution diffraction limit, solvent content and anomalous signal. This can allow a substantial reduction in the data-collection time required to determine a new structure. SAD phasing can therefore allow more structures to be solved for a given amount of synchrotron beamtime. This increased efficiency could prove useful for high-throughput structural genomics projects (reviewed by Kim, 1998).

None of our test data were collected at an undulator source at a third-generation synchrotron, where radiation damage is expected to be even more prominent. The reduced data-collection time required for SAD makes it a viable technique to use for radiation-sensitive crystals that would not be able to withstand the prolonged exposure of a full MAD experiment.

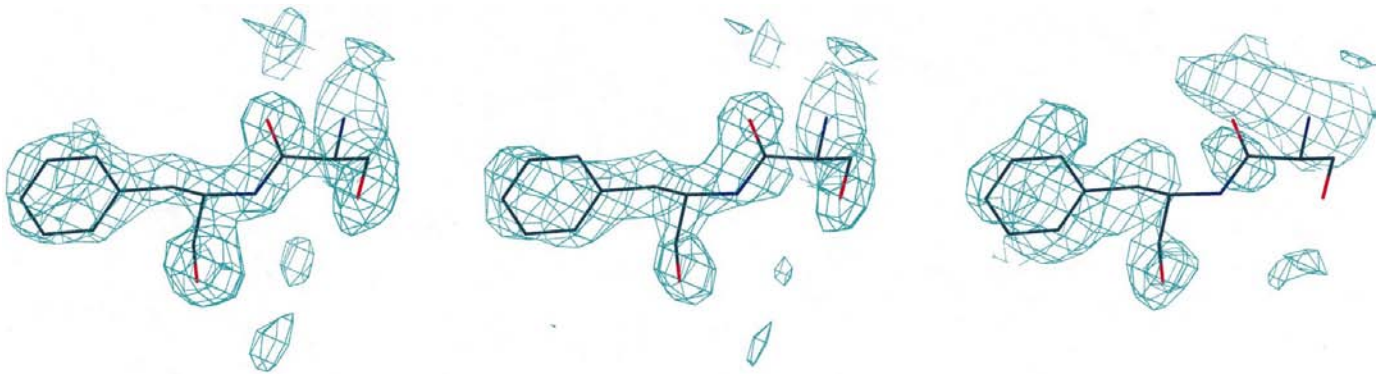

Figure 4
The effect of radiation damage on SAD phasing of 1qcs crystals. Representative electron density from the three SAD experiments using the same crystal. All maps were computed from the phases obtained using diffraction data processed to 2.0 Å resolution and are contoured at 1.25σ. From left to right, the maps correspond to data sets 1qcsc1, 1qcsc2 and 1qcsc3.

In particularly difficult cases, it is sometimes necessary to combine several independent MAD experiments in order to obtain interpretable maps (Sutton *et al.*, 1998). Our experiments with the 1sfc test case show that similar benefits can be obtained by combining independent SAD experiments. Furthermore, MAD beamlines are designed for wavelength tunability, which means that they can be sub-optimal for data collection at very high resolution or using very small crystals. SAD phasing could prove very useful for structure determinations under these experimental conditions.

Our experience and that of others (Peterson *et al.*, 1996; Evans & Wilson, 1999; Hendrickson & Ogata, 1997) is that the data-collection strategy is particularly important when attempting to derive phases from anomalous scattering. Typically, we collect anomalous diffraction data from all wavelengths in 15–20° wedges using inverse-beam geometry. We do not begin collecting the second wedge until the first wedge has been collected for all wavelengths. For the two MAD experiments which failed, 1qqe and 1qcsa, we used inverse-beam geometry and small wedges, but collected an entire wavelength before moving on to the next. The 1edu test case represents another extreme where the MAD phasing produced maps of exceptional quality while the SAD phasing failed; this was the result of crystal mis-centering during data collection.

Our results suggest that the combination of SAD phasing and solvent flattening will be sufficient to determine most structures. We recommend first collecting a complete diffraction data set at the peak anomalous wavelength, which should ensure optimally measured SAD data. Then, if sufficient synchrotron time is available and the crystal does not exhibit radiation decay, we recommend collecting further data sets to complete a MAD experiment. Care should be taken to minimize the effects of radiation damage, for example by using shorter exposures or an attenuated beam. Minimizing the absorbed dose could result in a slight loss of the highest resolution data, but we believe that this is preferable to the unpredictable effect of radiation damage. Furthermore, it is typically the case that additional crystals are available and could be used to collect higher resolution data for use in later refinement.

In summary, we believe that a phasing approach that combines accurately measured SAD data with density modification or direct methods will become an increasingly important tool for determining new macromolecular structures. This approach does not appear to require high-resolution diffraction, large anomalous signal or high solvent content. All of our test data sets came from selenomethionine-labelled crystals; however, as demonstrated by others, the phasing approach should be applicable to many different types of anomalous scatterers (Brodersen *et al.*, 2000; Dauter *et al.*, 1999; Dauter & Dauter, 1999). Indeed, SAD phasing was successful on the two test cases (1qcs and 1qqe) with the smallest anomalous signal. The most obvious applications for SAD phasing occur when either crystal decay is prominent or when the synchrotron beamtime or tunability is limited. It should also be noted that the SAD phasing approach can sometimes be successfully applied *a posteriori* in an attempt to derive useful phases from an otherwise failed MAD experiment.

We thank Richard Yu (1nsf and 1qcy), Bryan Sutton (1sfc), Danette Daniels (1kwa), Christian Ostermeier (1zbd) and Joel Hyman (1edu) for access to their MAD diffraction data. We also are grateful to Paul Adams for stimulating discussions, helpful advice and for critically reading the manuscript.

References

Abrahams, J. P. (1997). *Acta Cryst.* D**53**, 371–376.
Abrahams, J. P. & Leslie, A. G. W. (1996). *Acta Cryst.* D**52**, 30–42.
Bricogne, G. (1984). *Acta Cryst.* A**40**, 410–445.
Brodersen, D. E., de La Fortelle, E., Vonrhein, C., Bricogne, G., Nyborg, J. & Kjeldgaard, M. (2000). *Acta Cryst.* D**56**, 431–441.
Brunger, A. T., Adams, P. D., Clore, G. M., DeLano, W. L., Gros, P., Grosse-Kunstleve, R. W., Jiang, J.-S., Kuszewski, J., Nilges, M., Pannu, N. S., Read, R. J., Rice, L. M., Simonson, T. & Warren, G. L. (1998). *Acta Cryst.* D**54**, 905–921.
Burling, F. T., Weis, W. I., Flaherty, K. M. & Brunger, A. T. (1996). *Science*, **27**1, 72–77.

Burmeister, W. P. (2000). *Acta Cryst.* D**56**, 328–341.
Daniels, D. L., Cohen, A. R., Andersen, J. M. & Brunger, A. T. (1998). *Nature Struct. Biol.* **5**, 317–325.
Dauter, Z. & Dauter, M. (1999). *J. Mol. Biol.* **289**, 93–101.
Dauter, Z., Dauter, M., de La Fortelle, E., Bricogne, G. & Sheldrick, G. M. (1999). *J. Mol. Biol.* **289**, 83–92.
Doublie, S. (1997). *Methods. Enzymol.* **276**, 523–537.
Evans, G. & Wilson, K. S. (1999). *Acta Cryst.* D**55**, 67–76.
Garman, E. F. & Schneider, T. R. (1997). *J. Appl. Cryst.* **30**, 211–237.
Gonzalez, A., Pedelacq, J.-D., Sola, M., Gomis-Ruth, F. X., Coll, M., Samana, J.-P. & Benini, S. (1999). *Acta Cryst.* D**55**, 1449–1458.
Grosse-Kunstleve, R. W. & Brunger, A. T. (1999). *Acta Cryst.* D**55**, 1568–1577.
Hauptman, H. A. (1996). *Acta Cryst.* A**52**, 490–496.
Hendrickson, W. A. (1991). *Science*, **254**, 51–58.
Hendrickson, W. A., Horton, J. R. & LeMaster, D. M. (1990). *EMBO J.* **9**, 1665–1672.
Hendrickson, W. A. & Ogata, C. M. (1997). *Methods Enzymol.* **276**, 494–522.
Hendrickson, W. A. & Teeter, M. M. (1981). *Nature (London)*, **290**, 107–113.
Hendrickson, W. A. & Wüthrich, K. (1991–1999). Editors. *Macromolecular Structures.* London: Current Biology Publications.
Hyman, J., Chen, H., Di Fiore, P. P., DeCamilli, P. & Brunger, A. T. (2000). *J. Cell Biol.* **149**, 537–546.
Kim, S.-H. (1998). *Nature Struct. Biol.* **5**(Suppl.), 643–645.
Langs, D. A., Blessing, R. H. & Guo, D. (1999). *Acta Cryst.* A**55**, 755–760.
Ogata, C. M. (1998). *Nature Struct. Biol.* **5**(Suppl.), 638–640.
Ostermeier, C. & Brunger, A. T. (1999). *Cell*, **96**, 363–374.
Otwinowski, Z. & Minor, W. (1997). *Methods Enzymol.* **276**, 307–326.
Peterson, M. L., Harrup, S. J., McSweeney, S. M., Leonard, G. A., Thompson, A. W., Hunter, W. N. & Helliwell, J R. (1996). *J. Synchrotron Rad.* **3**, 24–34.
Phillips, J. C. & Hodgson, K. O. (1980). *Acta Cryst.* A**36**, 856–864.
Ravelli, R. B. G. & McSweeney, S. M. (2000). *Structure*, **8**, 315–328.
Read, R. J. (1986). *Acta Cryst.* A**42**, 140–149.
Rice, L. M. & Brunger, A. T. (1999). *Mol. Cell*, **4**, 85–95.
Sutton, R. B., Fasshauer, D., Jahn, R. & Brunger, A. T. (1998). *Nature (London)*, **395**, 347–353.
Walsh, M. A., Evans, G., Sanishvili, R., Dementieva, I. & Joachimiak, A. (1999). *Acta Cryst.* D**55**, 1726–1732.
Wang, B.-C. (1985). *Methods Enzymol.* **115**, 90–112.
Weik, M., Ravelli, R. B. G., Kryger, G., McSweeney, S., Raves, M. L., Harel, M., Gros, P., Silman, I., Kroon, J. & Sussman, J. L. (2000). *Proc. Natl Acad. Sci.* **97**, 623–628.
Yu, R. C., Hanson, P. I., Jahn, R. & Brunger, A. T. (1998). *Nature Struct. Biol.* **5**, 803–811.
Yu, R. C., Jahn, R. & Brunger, A. T. (1999). *Mol. Cell*, **4**, 97–107.
Zhang, K. Y. J. & Main, P. (1990). *Acta Cryst.* A**46**, 41–46.